Jang and Han, J Pollut Eff Cont 2018, 6:1
DOI: 10.4172/2375-4397.1000212

Journal of Pollution Effects & Control
ISSN: 2375-4397

Research Article Open Access

Production of Oxidant through Catalytic H_2O_2 Decomposition for NO Treatment

Jang JH and Han GB*

School of Chemical Engineering & Technology, Plant Engineering Center, Institute for Advanced Engineering, Republic of Korea

Abstract

The NO oxidation process has been applied to improve a removal efficiency of NO included in exhaust gas. In this study, to produce a dry oxidant for the NO oxidation process, the catalytic H_2O_2 decomposition method was proposed. A variety of the heterogeneous solid-acidic Mn-based catalysts were prepared for the catalytic H_2O_2 decomposition and the effect of their physico-chemical properties on the catalytic H_2O_2 decomposition was investigated. The results of this study showed that the acidic sites of the Mn-based catalysts have an influence on the catalytic H_2O_2 decomposition. The Mn-based catalyst having the abundant acidic sites within the wide temperature range in NH3-TPD shows the best performance for the catalytic H_2O_2 decomposition. Therefore, the NO oxidation efficiency, using the dry oxidant produced by the H_2O_2 decomposition over the Mn-based catalyst having the abundant acidic properties under the wide temperature range, was higher than the others. As a remarkable result, the best performances in the catalytic H_2O_2 decomposition and NO oxidation were shown when the Mn-based Fe_2O_3 support catalyst containing K component was used for the catalytic H_2O_2 decomposition.

Keywords: Mn-based catalyst; Catalytic H_2O_2 decomposition; Dry oxidant; NO oxidation

Introduction

NOx is a typical pollutant, which is produced through the combustion process of fossil fuels such as coal, petroleum, etc., and is discharged into the atmosphere [1]. Many researchers have conducted various studies to efficiently remove NOx, and a relatively widely applied technique is selective catalytic reduction (SCR) [2]. However, the selective catalytic reduction process requires a high temperature in order to increase the process efficiency while the catalyst is being applied. In the selective catalytic reduction process, NO is difficult to convert, which is a reason why a high temperature is required. Further, a process for oxidizing NO to NO_2 or the like is required to relatively easily process the NO. In this study, the decomposition of H_2O_2 catalysts, which can produce dry oxidants for the oxidation process to convert NO to NO_2, has been studied. Recently, a number of studies have been reported on various types of research results that can produce dry oxidants through H_2O_2 decomposition reaction on heterogeneous catalysts containing transition metals Fe and Zr as main components [3-5]. In addition, the H_2O_2 catalytic cracking reaction proceeds at a relatively low temperature to lower the operating temperature, and when the dry oxidant is applied to the oxidation process, the oxidation efficiency at a low temperature can be obtained [5]. It is believed that this simple facility can complement the disadvantages of the NO treatment process applied by the selective catalytic reduction method through the implementation of the process that can operate at low temperature with high efficiency [6-8]. In this study, H_2O_2 catalytic cracking was applied in order to convert the NO gas, which is difficult to process, into a dry oxidant that can be used simultaneously with the introduction of NO oxidation process. Therefore, the effect of the physico-chemical properties of the catalysts on the degradation of H_2O_2 catalysts was investigated by applying the catalysats having various physical properties in the H_2O_2 catalytic cracking process. The NO conversions characteristics were investigated. The reaction scheme for the production of dry oxidant by the decomposition of H_2O_2 using catalyst is shown in Equation (1), and the NO oxidation reaction formula is shown in (2) to (5) [9-11].

$$H_2O_2+M(II) \rightarrow \cdot OH+\cdot OH \quad (1)$$

$$NO+OH \rightarrow HNO_2 \quad (2)$$

$$NO+OH \rightarrow NO_2+H \quad (3)$$

$$NO+OH \rightarrow HNO_3 \quad (4)$$

$$NO_2+OH \rightarrow NO_3^-+H^+ \quad (5)$$

Experimental Method

Catalyst production

Figure 1 shows the process in which γ-Al_2O_3 is used as a carrier and the catalyst carrying Mn-based active material is prepared by the precipitation method. $Mn(NO_3)_2$ (reagent grade, Aldrich Co., 98% or more) was used as a precursor of the active material. A certain amount of $Mn(NO_3)_2$ was dissolved in distilled water in a beaker, and γ-Al_2O_3 as a carrier was mixed. Thereafter, precipitation process was carried out by dropping the NH_4OH solution as a precipitant until the pH value of the slurry mixture prepared in the above was within the range of 9 to 10. The precipitated mixture in the slurry state was aged by stirring in a bath at about 80°C for about 4 hours, then dried at 110°C for 24 hours and fired at about 700°C for 4 hours. The obtained Mn-based γ-Al_2O_3 catalyst, which is a solid product, was pulverized and the catalyst performance evaluation was carried out using a particle size ranging from about 100 to 150 μm through a sieving process. Figure 2 shows the preparation process of Mn-based catalyst with K component using Fe_2O_3 as a support. Fe_2O_3 (Powder, <5 μm, reagent grade, Aldrich Co., 98% or more) was used as a support. $KMnO_4$ (reagent grade, Aldrich Co., 98%) was used. First, the Fe_2O_3 support was mixed with distilled

***Corresponding author:** Gi Bo Han, School of Chemical Engineering & Technology, Plant Engineering Center, Institute for Advanced Engineering, Republic of Korea; Tel: +82313307408; Fax: +82313307111; Email: gbhan@iae.re.kr

Received June 10, 2017; **Accepted** January 25, 2018; **Published** January 30, 2018

Citation: Jang JH, Han GB (2018) Production of Oxidant through Catalytic H_2O_2 Decomposition for NO Treatment. J Pollut Eff Cont 6: 212. doi: 10.4172/2375-4397.1000212

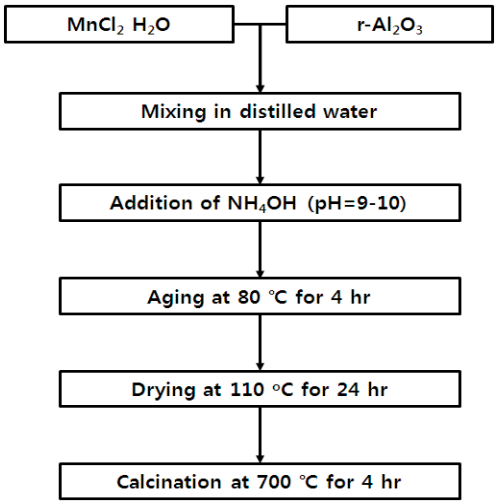

Figure 1: Preparation of Mn-Al_2O_3 catalysts.

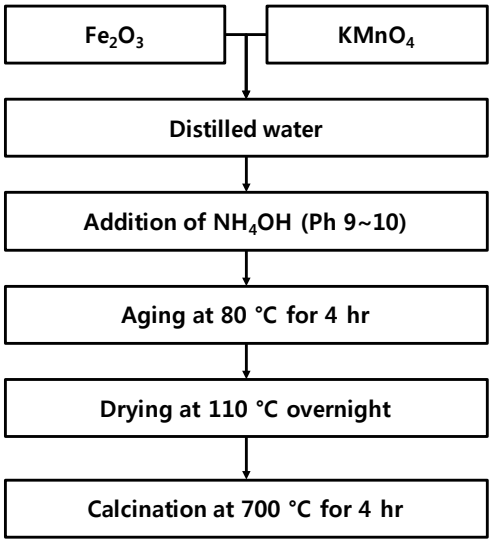

Figure 2: Preparation of K-Mn/Fe_2O_3 catalysts.

water through a mixing process to form a slurry state, and then mixed with a $KMnO_4$ aqueous solution as a precursor of the active material. The mixture was then dried at 110 DEG C for about 12 hours and then calcined at 700 DEG C for about 4 hours to produce a Mn-based Fe_2O_3 support catalyst with a K component added thereto.

For the preparation of SO_4^{2-}/ZrO_2 catalyst, Zr $(OC_3H_7)_4$ (reagent grade, Aldrich Co., 9 8% or more) was precipitated with ammonia water and dried at 110°C for 12 hours. The dried precipitate was mixed with 1 N H_2SO_4 Aging for 12 hours, drying at 120°C for 12 hours, and calcining at 500°C.

Analysis of catalyst characteristics

The effect of various physical and chemical properties of various catalysts on H_2O_2 decomposition was investigated by various techniques as follows. XRD analysis was performed to investigate the crystal structure and properties of the prepared catalysts. The quantitative and qualitative analysis of the elements constituting the catalysts was performed using EDX (Energy Dispersive X-ray Spectrometer for FE-SEM, FISONS Co., LEO SUPRA 55, GENESIS 2000 (Carl Zeiss, EDAX), and resolution: 138 eV/5B-92U. X-ray photoelectron spectroscopy (X-ray photoelectron spectroscopy, K-Alpha model) was used to analyse the qualitative and quantitative analysis of the sample surface and the chemical bonding state of the constituent elements. The temperature programmed desorption (TPD) experiment using NH_3 gas was conducted as follows to investigate the acidity characteristics of the heterogeneous catalysts prepared further. NH_3 gas having a concentration of about 10 volume % is filled in the catalyst bed for 6 hours. After the adsorption process is proceeded, N_2 gas is flowed and the temperature is increased from room temperature to 800°C at a rate of 5°C/min to be desorbed. The acid characterization was analysed by quantitative analysis of NH_3 with a thermal conductivity detector (TCD). In order to investigate the decomposition characteristics of H_2O_2 catalysts, 55 g of H_2O_2 and 0.1 g of the prepared catalyst were reacted on the balance. The weight change of H_2O_2 over time was recorded in 2 sec.

Decomposition of H_2O_2 and NO conversion experiment by type of catalyst

The experimental apparatus for evaluating the catalytic performance is composed of the H_2O_2 catalytic cracking process in which a dry oxidant is produced and the NO oxidizing process capable of oxidizing NO by injecting the dry oxidant prepared there from. The H_2O_2 catalytic cracking reaction, which can evaluate the catalytic performance, was carried out by passing H_2O_2 through an appropriate amount of flow rate together with the elevated temperature after a fixed amount of the catalyst was filled in the central portion of the tubular reactor of SUS material having an outer diameter of 1/2 inch. The reaction temperature was controlled through thermal transfer to the inside of the reactor using an automatic temperature controller after locating the heat conduction band (K-type) installed in the electric furnace at the same point as the catalyst filling layer. As the reactant, H_2O_2 (Duksan Co., 28-30%) to be decomposed was heated to be injected into the reactor in a vaporized state in the process of injecting the desired amount by using a metering pump. N_2 was then transferred by using it as carrier gas and injected into the tubular catalytic reactor after mixing in a chambered mixer. The gas used in the experiment was adjusted to the experimental parameters using a calibrated MFC (mass flow controller, Linetech Co.). At the rear end of the reactor, a condenser and an adsorbent loading layer were used to remove moisture at the end of the heat line. The H_2O_2 decomposition efficiency (%) was calculated by substituting into equation 6. The system for the NO oxidation process, which is connected to the downstream of the H_2O_2 catalytic cracking process, was constructed so that the dry oxidant produced by the H_2O2 decomposition and NO as the main reaction target can be simultaneously supplied at the desired concentration. In the NO oxidation process, a tubular reactor (material: SUS; outer diameter: 1/2 inch, length: 50 cm) filled with a fixed layer of bead type alumina having a diameter of 2.5 mm was used to increase the contact efficiency between the injected dry oxidant and NO gas) Was used. Reactivity experiments were carried out by simultaneously injecting dry oxidant and NO gas produced by the decomposition of H2O2 catalyst into the tubular reactor. At this time, NO was used for the gas composition of 1,000 ppm and N_2 was used as the dilution gas. The concentration values for the basic feed gas are shown in Table 1. The gas flow rate was controlled through a mass flow controller (Linetech Co.) with a calibrated MFC. The reaction conditions are shown in Table 2. Reactants and products were monitored by injecting every 5 min on-line to a gas chromatograph (DS science, Korea) equipped with a PDD (Pulsed Discharge Detector). In order to analyze NO and

Reactant gas	Composition
NO	1,000 ppm
Balance gas: N_2	-

Table 1: Basic composition in the gas bomb.

Factors	Values
Temperature	150°C
Space Velocity	36,000 cm^3/g-cat.·h
Input NO concentration	1,000 ppm

Table 2: Basic reaction conditions for the catalytic H_2O_2 decomposition.

NO_2 with G.C, a SUS separator filled with Hayesep Q was used. The detailed operating conditions for G.C are shown in Table 3. The NO conversion rate (% NO) to obtain the reactivity results was calculated by substituting the concentration of gases such as NO and NO_2 before and after the reaction into the equation (7) as follows.

$$H_2O_2 \text{ decomposition efficiency } (\%) = \frac{[H_2O_2]_{in} - [H_2O_2]_{out}}{[H_2O_2]_{in}} \times 100 \quad (6)$$

$$\text{NO conversion } (\%) = \frac{[NO]_{in} - [NO]_{out}}{[NO]_{in}} \times 100 \quad (7)$$

Results and Discussion

Characteristic analysis by catalyst

Table 4 shows the EDX analysis results for the constituents and their contents of K-Mn/Fe_2O_3, K-Mn/Al_2O_3, Mn/Al_2O_3 and ZrO_2 catalysts prepared for H_2O_2 decomposition. The K-Mn/Fe_2O_3 catalysts with K and Mn contents of about 30 and 70 weight %. In support Fe_2O_3 had Mn contents of 5.3 and 10.7 at.%, Fe contents of 17.3 and 10.3 at.%, Respectively, K component is present at about 3.6 and 8.1 at.%. The Mn/Al_2O_3 catalysts supported on Al_2O_3 support at 10, 30 and 70 weight %, Respectively, increased in the order of 3.5, 7.2 and 13.5% as the loading of Mn component increased. ZrO_2 and SO_4^{2-}/ZrO_2 catalysts according to surface treatment by sulphuric acid show that the Zr component corresponding to about 25~26 at.% is formed irrespective of surface treatment and the S component was not detected because the content was very small even though it was surface-treated. The amount of acid sites corresponding to the total NH_3 adsorption amount can be determined as an integrated value for a linear graph corresponding to the amount of desorbed NH_3 that varies with temperature. The total amount of acid sites for the NH_3 adsorption is Fe_2O_3<ZrO_2<10 wt.% Mn/Al_2O_3 and Lt; 30 wt.% Mn/Al_2O_3 & lt; K-Mn/Fe_2O_3. Figure 3 shows the intensity and distribution of acid sites along with the total amount of acid sites. As shown in Figure 4 and Table 5, the NH_3 desorption temperature corresponding to the acid strength corresponding to each catalyst is as follows. First, the ZrO_2 catalyst having the lowest acid amount has an acid point corresponding to a relatively low level of about 293°C, The amount of acid sites is also relatively low at 0.138 mmol/g. The 10 wt.% Mn/Al_2O_3 catalyst having a somewhat larger amount of acid sites than the ZrO_2 catalyst also has a total amount of acid sites of 0.889 mmol/g. However, the acid sites are at a desorption temperature of about 294°C as shown in Figure 5. On the other hand, the 30 wt.% Mn/Al_2O_3 catalyst with a few acid sites has relatively high acid sites ranging from about 270°C to 370°C and the acid sites are also 0.392 and 1.424 mmol/g. The K-Mn/Fe_2O_3 catalysts having relatively many acid sites have various acidic sites corresponding to about 217, 297, 355, 399, 452, 689, and 762°C and 1.337 mmol/g, respectively. The K-Mn/Fe_2O_3 catalyst rapidly undergoes electron transfer to determine the reaction rate during the H_2O_2 catalytic cracking reaction. This is due to the fact that the distribution of the Lewis acid sites in the catalyst phase, H_2O_2. It is because it exists in abundance. K is converted to ionic form after

Conditions	Values
Column material and length	Hysep Q (20 ft)
O.D.	1/8 inch
Carrier gas, flow rate	He, 30 cm^3/min
Column oven temperature	40~110°C
Injector temperature	110°C
Detector temperature	110°C

Table 3: Basic operation conditions of G.C.

Element	Content (at.%)						
	K-Mn/Fe_2O_3		Mn/Al_2O_3			ZrO_2	
	30wt.%	70wt.%	10wt.%	30wt.%	70wt.%	--	sulfated
Na	--	--	--	--	--	--	--
Al	--	--	16.5	13.2	10.1	--	--
Mn	5.3	10.7	3.5	7.2	13.5	--	--
Fe	17.3	10.3	--	--	--	--	--
K	3.6	8.1	--	--	--	--	--
Zr	--	--	--	--	--	25.9	26.1
O	73.8	70	53	65.4	53	73.1	73.9

Table 4: EDX analysis of the various catalysts for the catalytic H_2O_2 decomposition.

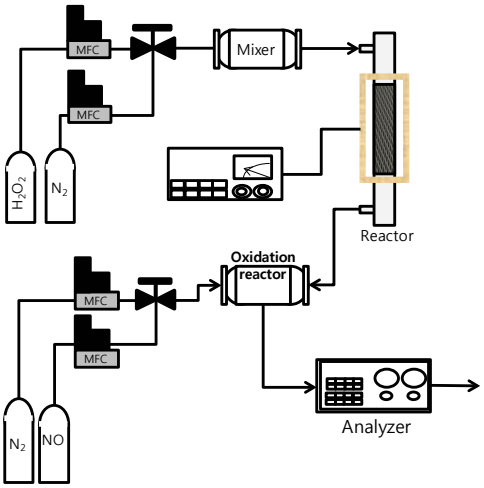

Figure 3: Schematic diagram of the experimental setup for catalytic H_2O_2 decomposition and NO oxidation.

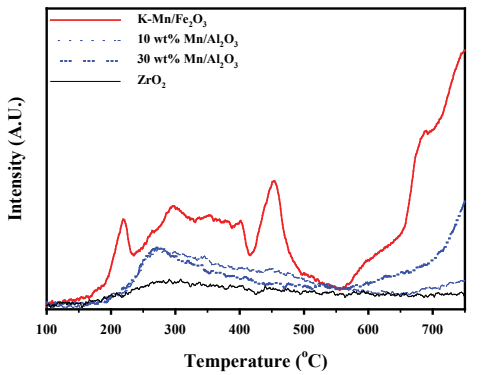

Figure 4: Acidic properties of the various catalysts by NH_3-TPD.

reduction and is placed on the carrier or Mn to change the electronic properties of Mn. When K is occupied by the active site of Mn, this active site is decreased and when the NH_3-TPD is observed, the acid

Catalysts		Peak No.	Max.Temp. (°C)	Quantity (mmol/g)
K-Mn/Fe_2O_3		1	217.7	0.066
		2	297.3	0.372
		3	355.5	0.212
		4	399.3	0.062
		5	452.7	0.225
		6	689.9	0.109
		7	762.9	1.337
Mn/Al_2O_3	10 wt.%	1	294	0.889
	30 wt.%	1	278.9	0.271
ZrO_2		2	771.6	0.245
		1	293.5	0.138

Table 5: Acidic properties of the various catalysts by NH_3-TPD.

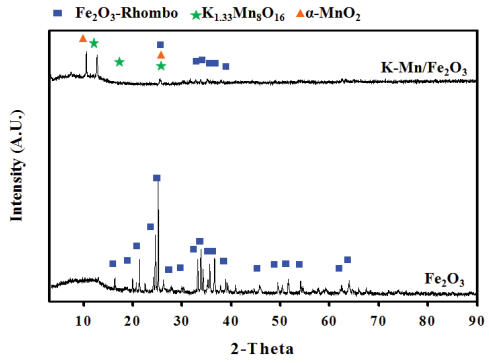

Figure 5: XRD analysis of the various catalysts.

concentration of the catalyst is weakened, so that the distribution of weak acid sites is increased [12]. It is also believed that it is advantageous for the H_2O_2 decomposition reaction because it is supposed to be due to the high electron and oxygen mobility due to the high oxidation state on the MnO_4 structure involved. In the case of using a catalyst based Al_2O_3 carrier-based MnO_2 catalyst, as the MnO_2 content is increased, the catalyst is converted into a relatively high oxidation state corresponding to Mn_2O_3, thereby improving the reactivity, but there is a limit to improve the catalyst performance And it is considered that there is a limit in the catalyst design to enrich the amount and intensity of the Lewis acid point mentioned above. As a result of the performance test of various catalysts containing Mn component, it is considered that the reactivity is low, and it is difficult to expect high activity due to low Mn content, which is the basic active substance on the decomposition of H_2O_2 catalyst. Especially, in case of $SO4_2$-/ZrO_2 catalyst, Although a strong acid point is expected, it is considered that it is not suitable for the decomposition of H_2O_2 catalyst due to low performance because it corresponds to the kind of Brönsted acid sites at the same time as the absence of Mn component as a basic active material. Figure 5 shows the XRD analysis results for Fe_2O_3, Al_2O_3, K-Mn/Fe_2O_3, and Mn/Al_2O_3 catalysts. Fe_2O_3 catalyst was found to have crystallinity of rhombohedrol structure. On the K-Mn/Fe_2O_3 catalyst prepared by using it as a support, Fe_2O_3 of rhombohedrol structure exists and at the same time, K1.33Mn8O16 compound form and α-MnO2 compound form. Al_2O_3 is present as a γ-Al_2O_3 compound. On the Mn/Al_2O_3 as a support, γ-Al_2O_3 and K1.33Mn8O16 type compounds are present at the same time, and α-MnO_2 compound is not present. Figure 6 shows the results of XRD analysis of Mn/Al_2O_3 catalyst prepared by supporting Al_2O_3 and Mn as support. Al_2O_3 is present as a compound of γ-Al_2O_3 type. In the case of 10 wt.% Mn/Al_2O_3 catalyst containing 10 wt.% Mn as a support, the morphology of MnO_2 compound is added by XRD analysis As shown in Figure 7. In the case of the 30 wt.% Mn/Al_2O_3 catalyst, γ-Al_2O_3-type compounds and Mn_2O_3-type compounds were present. MnO_2 and α-Mn_2O_3-type compounds could not be confirmed by XRD analysis. As a result, it can be seen that, when the Mn component is supported on the Al_2O_3 support, the Mn component is converted into another oxidation state compound as the Mn content increases. This is because the oxidation, and the oxidation state of the Mn component, which is an active material, is considered to be a major influential factor. Figure 7 shows the XRD analysis of the $SO4_2$-/ZrO_2 catalyst prepared by treating the surface with ZrO_2 catalyst and sulphuric acid. As a result, it can be understood that ZrO_2 catalyst is a ZrO_2 compound having monoclinic and tetragonal structures coexisting. In case of SO_4^{2-}/ZrO_2 catalyst surface treated with sulphuric acid, it is difficult to bring about crystal change of sulphate functional group and related ZrO_2 compound itself Changes in structure and related characteristics cannot be confirmed.

Figure 8 shows the results of XPS analysis of the binding energy of elemental components to confirm the binding state of constituent elements of K-Mn/Fe_2O_3 catalyst supporting K and Mn in support Fe_2O_3. As shown in Figure 8a, the binding energy of the Mn component was obtained in various peaks, but at binding energies corresponding to about 642.2 and 654.1 eV. The type of compound containing Mn component corresponding to this binding energy position is $KMnO_4$. Figure 8b also shows the binding energy of the K component, which is 292.6 eV, indicating the binding structure of K and $KMnO_4$. The bond energy for the Fe component shown in Figure 8c was two peaks corresponding to about 710.05 and 723.5 eV, and this binding energy was found to be the binding energy of the Fe component contained

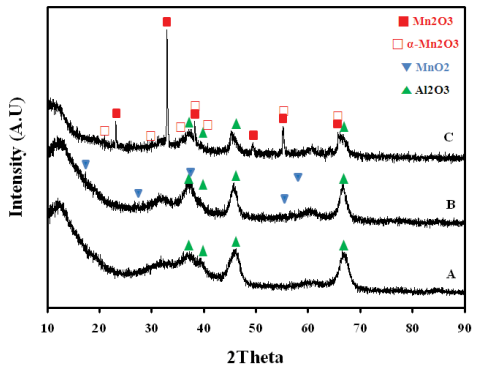

Figure 6: XRD analysis of the various catalysts (A: Al_2O_3, B: 10 wt.% Mn/Al_2O_3, C: 30 wt.% Mn/Al_2O_3).

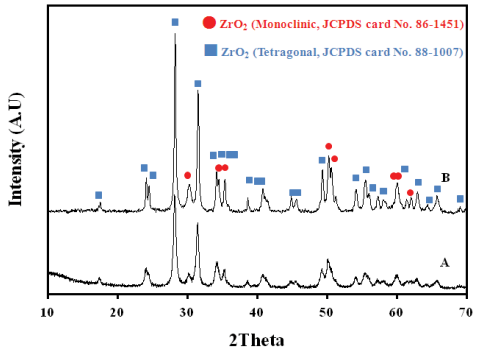

Figure 7: XRD analysis of the various catalysts (A: ZrO_2, B: SO_4^{2-}/ZrO_2).

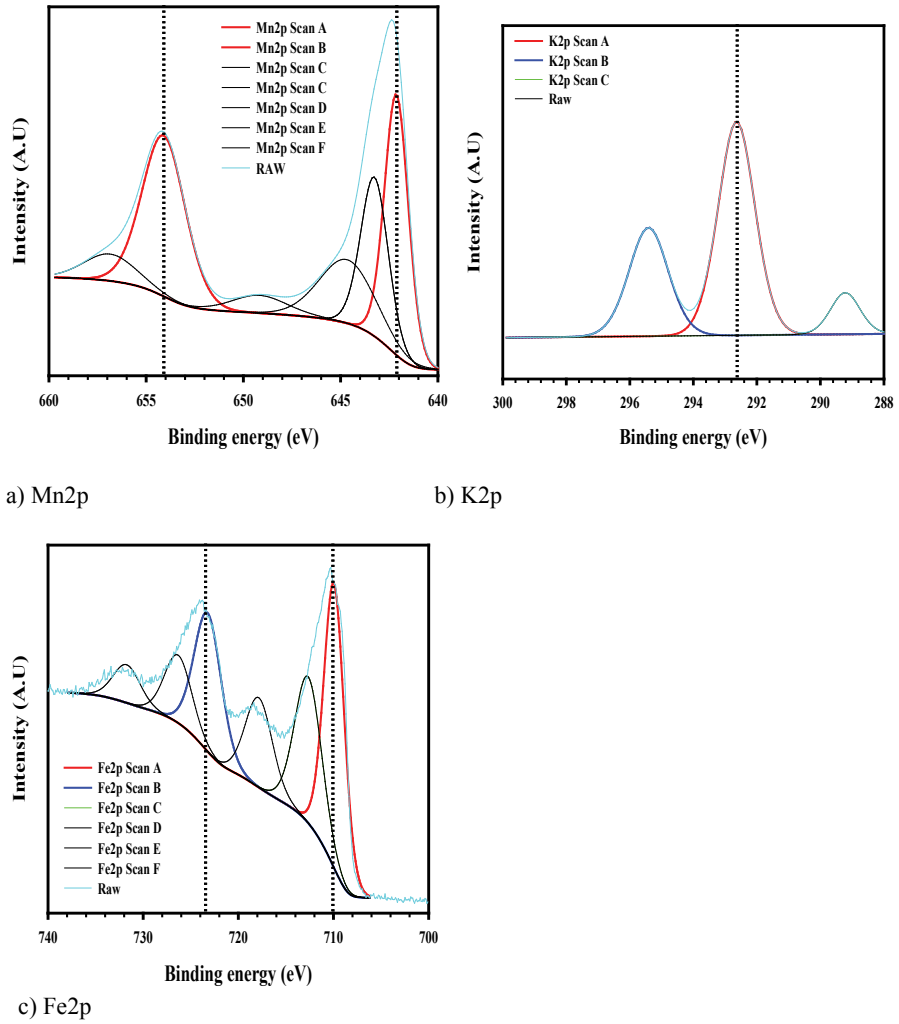

Figure 8: XPS analysis of Fe_2O_3 & K-Mn/ Fe_2O_3 catalysts.

in the Fe_2O_3 compound. Therefore, it is considered that the property of K-Mn/Fe_2O_3 catalyst is composed of Fe_2O_3 which is a support, mostly containing $KMnO_4$ component. Figure 9 shows the results of XPS analysis of the binding energy of constituent elements for the 10 wt.% Mn/Al_2O_3 catalyst prepared by loading 10 wt.% Of Mn on the support γ-Al_2O_3. As shown in Figure 9a, the binding energy of the Mn component is about 641.8 and 653.8 eV, indicating that the main Mn compound with such binding energy is MnO_2. The bond energy for the Al component contained in Al_2O_3, another component, was obtained at 73.9 eV as a single peak and is shown in Figure 9b. It can be seen that such a peak position is maintained as a support of the compound type introduced before production as the Al_2O_3 compound. Figure 10 shows the results of XPS analysis of the binding energy of the constituent elements for the 70 wt.% Mn/Al_2O_3 catalyst loaded with Mn on support Al_2O_3. Figure 10a shows a relatively large number of binding energy peaks as compared to the above-mentioned 10 wt% Mn-supported catalyst. As Mn content increases, various Mn compounds are formed in addition to MnO_2 Able to know. However, the peaks corresponding to 641.7 and 652.8 eV were observed at the positions of the most important binding energies, respectively, and this binding energy tendency can be obtained as a result of the MnO_2 compound. In Figure 10b, the binding energy position for the Al component is 73.6 eV, which means that it is present as a typical Al_2O_3 compound. Based on these results, it is considered that the Mn component is present in the MnO_2 phase and the catalyst supported on Al_2O_3 is supported. As shown in Figure 11, the position of the peak corresponding to the bonding energy of the Zr component is 186.5 eV regardless of whether the surface treatment is performed or not. As can be seen in Figure 11, the peak position of the binding energy for the S component present in the SO_4^{2-}/ZrO_2 catalyst surface treated with sulfuric acid is about 168.8 eV. This means that SO_4^{2-}functional groups are formed on the surface of ZrO_2 due to surface treatment with sulfuric acid as binding energy corresponding to formation of SO_4^{2-}functional group. These SO_4^{2-}functionalized catalysts are known to enhance the catalytic effect in reactions involving related reaction mechanisms by further enhancing the strength and quantity of acid sites.

Decomposition of H_2O_2 and NO conversion according to the type of catalyst

Mn/Al_2O_3>10 wt.% Mn/Al_2O_3 catalyst was used as a catalyst. The results showed that the decomposition efficiency of H_2O_2 by the catalyst was K-Mn/Fe_2O_3 and Mn/Al_2O_3>Fe_2O_3>SO_4^{2-}/ZrO_2. The decomposition

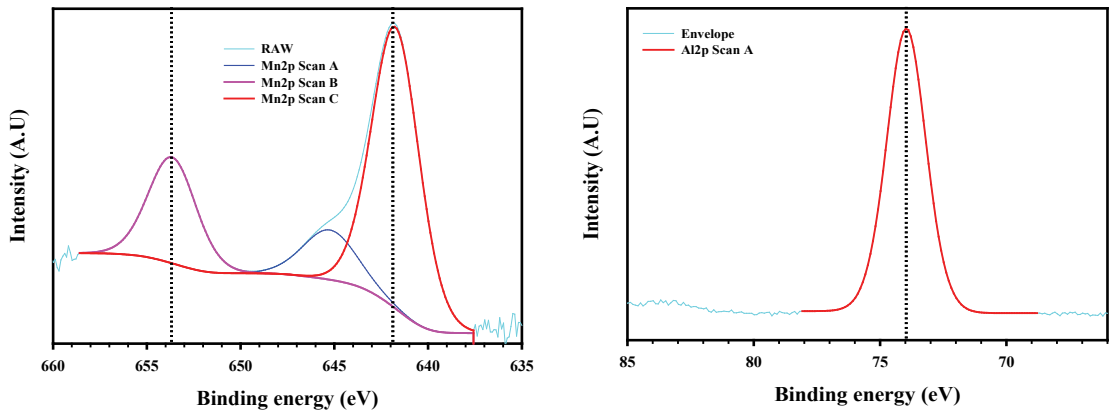

a) Mn2p b) Al2p

Figure 9: XPS analysis of 10 wt.% Mn/Al_2O_3 catalysts.

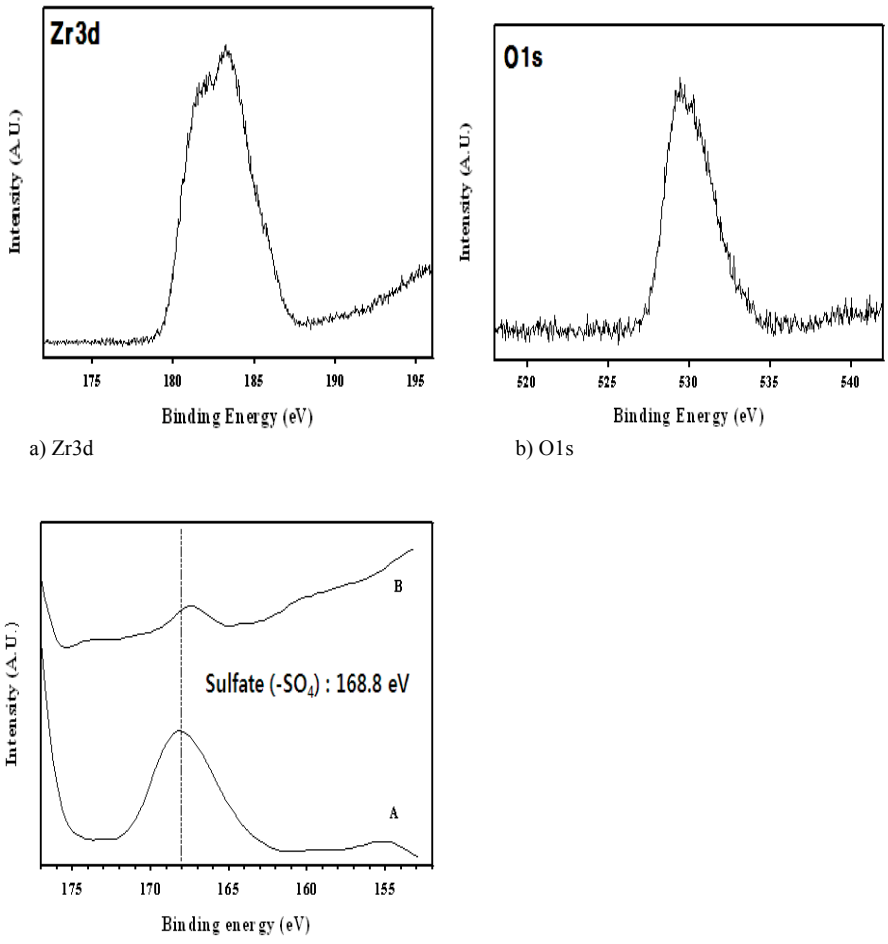

a) Zr3d b) O1s

c) S2p

Figure 10: XPS analysis of SO_4^{2-}/ZrO_2 catalysts (A: Before sulphuric acid treatment, B: after sulphuric acid treatment)

rate of H_2O_2 varies depending on the type of active material and the amount of dry oxidant generated at that time varies [13-15]. Figure 12 shows the conversion efficiency as H_2O_2 decomposition efficiency depending on the type of catalyst performed for the production of dry oxidant.

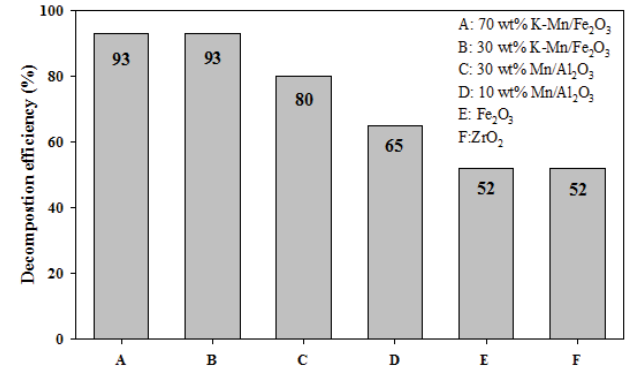

a) H_2O_2 Decomposition efficiency (%)

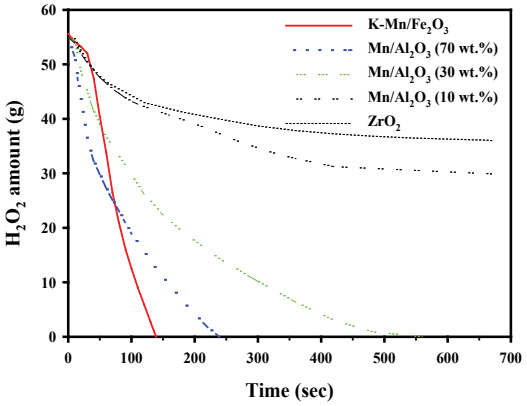

b) H_2O_2 amount (g)

Figure 11: Effect of the various catalysts on the catalytic H_2O_2 decomposition.

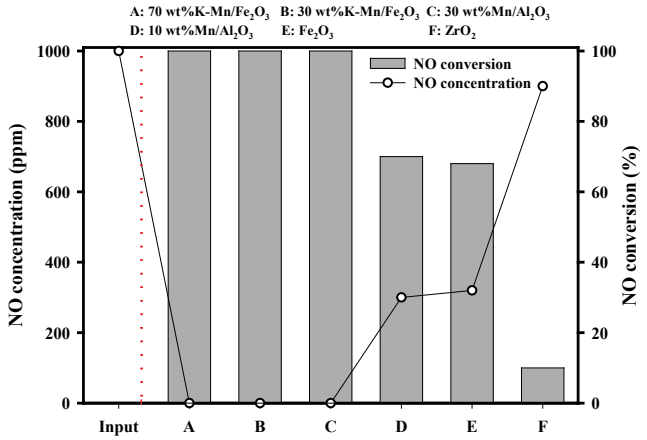

Figure 12: Effect of the various catalysts on NO oxidation.

These results are strongly influenced by the distribution of the acid sites of the catalysts, which are most related to the characteristics of the H_2O_2 decomposition reaction, among the physicochemical properties of the various catalysts produced. H_2O_2 decomposition reaction characteristics are dependent on the oxidation-reduction reaction due to electron mobility, and the reaction characteristic is related to the Lewis acid point of the solid catalyst. In addition, it is considered that the size of reactivity depends on the distribution and amount of weak acid sites in the characteristics of H_2O_2 as a reaction target in the acid sites. Figure 11 shows the amount of decomposition of H_2O_2 by decomposition of H_2O_2 catalyst by type of catalyst for the production of dry oxidant. The catalysts used were 10, 30, and 70 wt.% Mn/Al_2O_3 catalysts and SO_4^{2-}/ZrO_2 catalysts, which were different in content from K-Mn/Fe_2O_3 catalysts. As a result, it was found that the decomposition efficiency of H_2O_2 gradually increased with time regardless of the kind of catalyst, and it was found that the time required for stabilizing the decomposition efficiency of H_2O_2 catalyst, that is the order of magnitude of reactivity was as follows: K-Mn/Fe_2O_3>70 wt.% Mn/Al_2O_3>30 wt.% Mn/Al_2O_3>10 wt.% Mn/Al_2O_3>SO_4^{2-}/ZrO_2. The same tendency as the test result was obtained. To investigate the characteristics of the NO oxidation reaction proceeding in the downstream oxidation process by using the dry oxidant prepared according to the decomposition reaction characteristics of the performed H_2O_2 catalysts. Figure 12 shows the NO conversion efficiency (value in the graph, in%) by injecting the dry oxidant obtained after the H_2O_2 decomposition reaction carried out according to the above catalyst type into the oxidation process together with the exhaust gas. The reaction temperature was controlled at 150°C and the amount of H_2O_2 injected and the amount of catalyst loaded were 0.3 g/min and 0.5 g respectively. The oxidation process also controlled the reaction temperature to 150°C, and the flow rate of injected simulated flue gas and NO concentration were 300 ml/min and 1,000 ppm respectively. The conversion efficiency of NO in the oxidation process varied depending on the type of catalyst, and the NO conversion rate varied depending on the performance of the catalyst obtained in the H_2O_2 decomposition process. As a result, the NO conversion efficiency of the catalysts used in the H_2O_2 decomposition process was K-Mn/Fe_2O_3 and Mn/Al_2O_3 catalysts, and the conversion of NO obtained in the oxidation process reached about 100%. The NO conversion rates of the catalysts used in the H_2O_2 decomposition process were K-Mn/Fe_2O_3≈Mn/Al_2O_3>>30 wt.% Mn/Al_2O_3>10 wt.% Mn/Al_2O_3>Fe_2O_3>SO_4^{2-}/ZrO_2 And so on.

Conclusion

In this study, the conversion of dry oxidant obtained from H_2O_2 catalytic cracking was investigated by injecting the dry oxidant obtained from it into the subsequent NO oxidation process. First, various catalysts were prepared and applied to H_2O_2 decomposition reaction. As a result, it was found that the acid sites possessed by the catalyst had the greatest effect on the decomposition efficiency of H_2O_2, and the acid sites present on the catalyst surface were uniformly distributed from weak acid sites to strong acid sites. The H_2O_2 decomposition efficiency was higher. Also, when the dry oxidant obtained from this process was injected into the NO oxidation process, the NO conversion efficiency was increased as the decomposition efficiency of H_2O_2 was increased. Therefore, Mn-based Fe_2O_3 catalyst with K component as the catalyst having a uniform and rich acid point ranging from the weakest point to the strongest point among the various catalysts produced showed the highest decomposition efficiency of H_2O_2, The NO conversion rate obtained under optimized operating conditions on the NO oxidation process using dry oxidant reached about 100%.

Acknowledgment

This study was supported by the Ministry of Environment's environmental industry advancement technology development project.

References

1. Qi G, Yang RT (2003) Low-temperature selective catalytic reduction of NO with NH_3 over iron and manganese oxides supported on titania. Appl Catal B 44: 217-225.

2. Dahiya RP, Mishra SK, Veefkind A (1993) Characterization and performance comparison of ripple-based control for voltage regulator modules. IEEE Trans Plasma Sci 21: 346-348.
3. Lin SS, Gurol (1998) Catalytic decomposition of hydrogen peroxide on iron oxide: Kinetics, mechanism and implications. Environ Sci Technol 32: 1417-1423.
4. Lousada CM, Jonsson (2010) Kinetics, mechanism and activation energy of H_2O_2 decomposition on the surface of ZrO_2. J Phys Chem C 114: 11202-11208.
5. Pham ALT, Lee C, Doyle FM, Sedlak DL (2009) A silica-supported iron oxide catalyst capable of activating hydrogen peroxide at neutral pH values. Environ Sci Technol 43: 8930-8935.
6. Adewuyi YG, Owusu SO (2006) Ultrasound-induced aqueous removal of nitric oxide from flue gases: effects of sulfur dioxide, chloride, and chemical oxidant. J Phys Chem A 110: 11098-11107.
7. Ding J, Zhong Q, Zhang S, Song F, Bu Y (2014) Simultaneous removal of NOX and SO_2 from coal-fired flue gas by catalytic oxidation-removal process with H_2O_2. Chem Eng J 243: 176-182.
8. Ding J, Zhong Q, Zhang S (2014) Simultaneous removal of NO_x and SO_2 with H_2O_2 over Fe based catalysts at low temperature. RSC Advances 4: 5394.
9. Mauldin RL, Kosciucha E, Henrya B, Eiselea FL, Shettera R (2004) Measurements of OH, HO_2+RO_2, H_2SO_4, and MSA at the south pole during ISCA 2000. Atmos Environ 38: 5423-5437.
10. Thomas D, Vanderschuren J (1997) Modeling of NO_x Absorption into nitric acid solutions containing hydrogen peroxide. Ind Eng Chem Res 36: 3315-3322.
11. Park SY, Deshwal BR, Moon SH (2008) NO_x removal from the flue gas of oil-fired boiler using a multistage plasma-catalyst hybrid system. Fuel Process Technol 89: 540-548.
12. Fang D, Xie JL, Hu H, Zhang Z, He F, et al. (2015) Effects of precursors and preparation methods on the potassium deactivation of MnO_x/TiO_2 catalysts for NO removal. Fuel Processing Technology 134: 465-472.
13. Hermanek M, Zboril R, Medrik I, Pechousek J, Gregor C (2007) Catalytic efficiency of Iron (III) oxides in decomposition of hydrogen peroxide: Competition between the surface area and crystallinity of nanoparticles. J Am Chem Soc 129: 10929-10936.
14. Choudhary VR, Samanta C, Jana P (2007) Hydrogenation of hydrogen peroxide over palladium/carbon in aqueous acidic medium containing different halide anions under static/flowing hydrogen. Ind Eng Chem Res 46: 3237-3242.
15. Schmidt HF, Meuris M, Mertens PW, Rotondaro ALP, Heyns MM, et al. (1995) H_2O_2 decomposition and its impact on silicon surface roughening and gate oxide integrity. Jap J Appl Phys 34: 727-731.